# Nanoscale

Accepted Manuscript


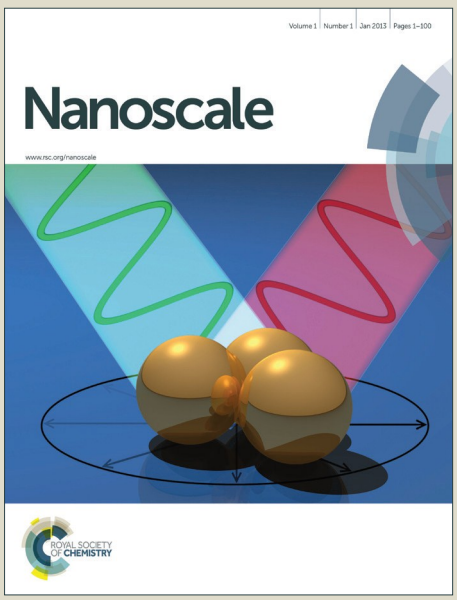





ROYAL SOCIETY OF CHEMISTRY

www.rsc.org/nanoscale

# Ultra-large suspended graphene as highly elastic membrane for capacitive pressure sensor

Yu-Min Chen [†#], Shih-Ming Ho[#], Chi-Hsien Huang [$] Cheng-Chun Huang[^], Wen-Pin Shih[^] , Chun-Lin Chu[&], Jing Kong[+], Ju Li[@] and Ching-Yuan Su [†#%*]

[#] *Graduate Institute of Energy Engineering, National Central University, Tao-Yuan 32001 , Taiwan*

[†] *Dep. of Mechanical Engineering, National Central University, Tao-Yuan 32001 , Taiwan*

[$] *Dep. of Materials Engineering, Ming Chi University of Technology, New Taipei City 24301, Taiwan*

[^] *Dep. of Mechanical Engineering, National Taiwan University, Taipei City 10617, Taiwan*

[&]*National Nano Device Laboratories, Hsinchu, 30078 ,Taiwan*

[+] *Department of Electrical Engineering and Computer Sciences, Massachusetts Institute of Technology, 77 Massachusetts Avenue, Cambridge, MA 02139, USA*

[@]*Department of Nuclear Science and Engineering and Department of Materials Science and Engineering, Massachusetts Institute of Technology, Cambridge, Massachusetts 02139, USA*

[%] Graduate Institute of Material Science and Engineering, National Central University, Tao-Yuan 32001 , Taiwan

To whom correspondence should be addressed: (C. Y. Su) cysu@ncu.edu.tw

**KEYWORDS**: Suspended graphene, graphene, pressure sensor, chemical vapour deposition, 2D materials

## Abstract

In this work, we fabricate ultra-large areas of suspended graphene membranes, where the stacking of a few layers of graphene could be suspended over a circular hole of diameter upto1.5 mm, with a diameter to thickness aspect ratio of $3x10^5$,which is the record for free-standing graphene membranes. The process is based on large crystalline graphene(~55μm) obtained from the chemical vapor deposition(CVD) method, followed by a gradual solvent replacing technique. Combining a hydrogen bubbling transfer approach with thermal annealing to reduce polymer residue result in an extremely clean surface, where the ultra-large suspended graphene preserves the intrinsic features of graphene, including phonon response and enhanced carrier mobility(200% higher than that of graphene on a substrate). The highly elastic mechanical properties of graphene membrane is demonstrated, and the Q-factor under 2 MHz stimulation is measured to be 200-300.Agraphene-based capacitive pressure sensor is fabricated, where it shows a linear response and a high sensitivity of 15.15 aF/Pa, which is 770% higher than that of frequently used silicon-based membranes. The reported approach is universal, which could be employed to fabricate other suspended 2D materials towards macro scale sizes on versatile support substrates, such as arrays of Si nano-pillars and deep trenches.

## Introduction

The freestanding 2D membrane represents an new functions to materials and devices. For example, the reported works demonstrate the suspended highly ordered and elastic membranes by self-assembly of nanomaterials such as nanoparticle or nanowire, which shows potentials on nanodevices and sensor applications.[1-5] Graphene, an atomic layer of graphite, has attracted intensive interests in the last decades.[6] The earlier studies on graphene were usually performed on supporting substrates such as $SiO_2$/Si. However, substrate induced carrier scattering, dopants and phonon leakage significantly obscured the intrinsic properties of graphene. Recent studies on suspended graphene have revealed superior physical and chemical properties, and have provided ultimate platforms for exploiting the properties of pristine graphene, such as the extremely high carrier mobility (~200 000 $cm^2$/Vs),[7] high mechanical strength (~130GPa),[8] and superior thermal conductivity(~5300 W/mK)[9]. All of these unique properties have spurred various fundamental research topics, including the atomic layer mechanics,[10-12] electronic transport, and heat propagations.[13] Additionally, suspended graphene has been proposed for many exciting applications in future technologies, such as electromechanical resonators/actuators, [14] higher performance biological membranes, sensors for DNA sequencesand cancer detection, [15, 16] piezoresistive pressure sensors, [17] bright visible light emissions,[18] high responsivity photodetectors, [19] gas impermeable membranes or permeance membranes for gas, liquid or molecular separation,[20 21] and high resolution TEM imaging on wet biological samples. [22-25] Most of these potential applications require large-area, extremely thin(<10 nm), and residue-free membranes, therefore suspended graphene is an ideal candidate in this regard. However, there is still no reliable approach to prepare suspended graphene on a macro-scaled size, i.e., larger

than the millimeter scale, mainly due to the rupture force on the graphene membrane from the surface tension of liquid during wet-etching and drying procedures. The obtained size based on the conventional approach is limited to a few micrometers in diameter.[26, 27] In recent works for obtaining free-standing graphene membranes, the graphene was first transferred to the substrate, followed by critical point drying to avoid the drag force from surface tension.[12, 28] With this approach, the size could be improved to a few tens of micrometers. However, this size is still limited for most applications, and an additional issue is the introduction of unwanted impurity and residue on the graphene surface by employing this drying method. In 2014, Lee et.al., published a strategy called inverted floating method in which acetone is gradually replaced by a solvent with a low surface tension to lower the drag force when drying, resulting in a suspended graphene membrane with up to ~500μm in diameter.[29] However, it was found to suffer from the large amount of polymer residue on the graphene surface. This residue issue is crucial for specific applications, such as chemical/bio-medical sensors, that require an extremely clean graphene surface for ultra-sensitive sensing. Therefore, the development of large scale, free-standing, and clean graphene membranes for the aforementioned applications is of great importance.

Suspended graphene membranes have been demonstrated to be promising materials for electromechanical piezoresistive pressure sensors, which show orders of magnitude greater sensitivity than other membrane materials, such as silicon and carbon nanotubes (CNTs).[17] Recently, capacitive pressure sensors have been intensively investigated because of their widespread applications in medicine, aerospace, and automobile due to the advantages of high sensitivity, low temperature dependence, higher signal response and lower power consumption when compared to piezoresistive-type sensors. In general,

the high sensitivity of a capacitive pressure sensor requires (1) a larger membrane area,(2) a reduced membrane thickness, and (3) a decreased sensing gap. [30] Therefore, suspended graphene membrane is the ideal candidate in this regard.

In this work, we demonstrate a novel method to yield the largest(up to 1.5 mm) and highest quality suspended graphene membranes by solvent replacement, followed by thermal decomposition. X-ray photoelectron spectrometer (XPS) characterization shows an extremely clean graphene membrane with low oxygen functional groups (4～6%). To demonstrate a potential application based on this ultra-large suspended graphene, a pressure sensor was created. The as-prepared graphene-based capacitive pressure sensor shows a sensitivity of 15.15 aF/Pa, which is 770% higher than that of conventional silicon-based materials made by micro-fabrication technologies. This study sheds light on the development of atomic layered devices and addresses the present bottleneck to bridge applications from the nano- to the macro-scale, while preserving the high performance intrinsic properties of graphene. Additionally, the ultra-large freestanding graphene or other 2D layered membranes could be applied as an ideal platform to exploit new chemical/physical phenomena down to the atomic layered scale.

**Results and Discussion**

The graphene film used in this work was synthesized by an atmosphere pressure CVD (APCVD) method(see the Experimental Section for detail).To obtain high mechanical strength graphene films for the subsequent fabrication of suspended membranes, graphene sheets with large single crystalline domains were obtained by

comprehensively studying and optimizing the growth process conditions(see S1). Figure 1a shows the SEM image for a graphene domain, where the denoted white-line is the defined lateral size of a single crystalline domain. Figure 1b shows the statistical analysis of the graphene domain size according to various growth conditions. The results clearly reveal that the three conditions of 1045℃ with $H_2$=20 sccm and 1060℃with $H_2$=20 and 30 sccm yielded relatively large domain sizes. Subsequently, continuous graphene films were obtained by extending the growth time based on these three conditions. The as-grown samples were further characterized by Raman spectroscopy and Hall measurements to verify the quality. Figure 1c shows the Raman spectra for these three samples, where the case of 1060℃/$H_2$=20 shows a lower D/G intensity ratio, indicating a low defect density. Further characterization of the AFM height profile(~0.78nm in Figure 1d) and cross-section TEM for the sample(Figure S2) shows a uniform single-layered graphene film. In addition, the sheet resistance and optical transparency were characterized (see Figure S1-3), exhibiting the lowest sheet resistance of 592 ohm/sq at an optical transmittance of ~97%, suggesting a single layered graphene and a lower density of the graphene boundary in the obtained film. Thus, the following suspended graphene membranes in this study were synthesized by this condition.

The detailed procedure in fabricating the suspended graphene samples can be found in the Experimental Section. Briefly, the five-layered(5L) graphene was made by layer-by-layer stacking, and then it was transferred onto substrates with holes using supporting polymethyl methacrylate (PMMA) layers, where the hole diameters ranged from few tens of micrometers to two millimeters(Figure2a).It is clearly observed that

the graphene/PMMA composite film remained well-suspended over the holes without rupturing, mainly due to the high strength of the supporting PMMA layers(Figure2b).

Unlike previous works where the PMMA layer was removed with acetone causing the graphene film to easily rupture when the solution dried, a solvent replacing approach was employed in this study. Figure 2c illustrates the experimental setup, where the sample faced down and bridged on a channel. Acetone was gradually streamed into the channel, and the PMMA layer was then removed when the flow contacted the surface. After 10 min, the solution was switched from acetone to a low surface tension solvent, i.e., methoxynonaflurorbutane ($C_4F_9OH_3$). It was found that the 5L graphene membrane could suspend over the substrates with holes of diameters ranging from 200μm up to 1.5 mm, as shown in Figure 2d.To prevent the rupture of the membrane, the drag force, induced during the solvent drying process, needs to be considered and depends on a combination of quite a few factors, such as density, viscosity, velocity etc., and among them, the surface tension is regarded as the dominant factor. Therefore, it is of great importance to further examine the surface tension. Figure S3 shows the contact angle measurements, where the contact angles are Water($89.58^o$), Acetone ($13.52^o$),and $C_4F_9OH_3$($10.57^o$), indicating that a lower surface tension can significantly lower the drag force and does not lead to the rupture of the suspended graphene membrane when drying.

Note that the suspended membrane of a single layer graphene was limited to approximately 600 μm in hole diameter by the same process. In the case of 1.5 mm hole, it was found out that the stacking layers ranged from 1~4 layers were unable to obtain a

fully-coverage film without rupturing, indicating the stacking of up to five layers of graphene can provide sufficient mechanical strength to compensate the rupture force arising from the surface tension of the solvent. Figures 3a and b show the Raman spectra for the single-layered suspended graphene and the substrate-supported single-layered graphene, where a narrow band width of 33 $cm^{-1}$ and the down shifting of G and 2D bands were clearly observed in the suspended graphene sample. This result indicates that the graphene is free from the interaction from the substrate, and this feature is consistent with the reported works on suspended graphene films.[31]

By employing the solvent replacing method for 5-layered graphene, it was found that the largest suspended graphene membranes over 1.5 mm diameter holes can be successfully obtained as shown in Figure 3c(the yield rate is ~10%). To our best knowledge(see Table S7 for this comparison), this was the largest suspended graphene membrane. In addition to the solvent replacing method, a direct thermal decomposition approach was carried out for preparing suspended graphene membranes, where the samples were subjected to thermal annealing under a fuming gas atmosphere($H_2$/Ar) to remove the PMMA supporting layers(see Experimental Section). In this case, the yield rate (for a 1.5 mm diameter hole) was doubled compared to that from the solvent replacing method, indicating that the direct sublimation to decompose PMMA polymer could be a more reliable method for yielding large-area suspended graphene. Figure 3d shows the statistical analysis of the yield rate for these two methods, indicating the significantly increased yield rate for the thermal decomposition approach, especially for large holes with diameters ranging from 600 to 1500 μm.

However, by employing the thermal decomposition method, it was found that the unwanted non-crystalline phase of carbon appeared on the as-prepared graphene surface. Figure 4a shows the typical Raman spectra for the suspended graphene made by three different approaches. The pronounced broad peak between the G and D bands was clearly seen for the sample made by direct thermal annealing, which was due to the non-crystalline carbon phase as denoted by amorphous carbon (α-C) in the spectrum. This was attributed to the carbonization of polymer from the thick PMMA layer during the thermal decomposition process, where the PMMA directly transforms to α-C and remains on the graphene surface rather than a gradual sublimation.

Moreover, the XPS characterization shows that 36.6 % of oxidized functional groups(mainly C-O, C=O and O-C=O)were on the surface(Figure 4b). The existence of a large amount of unwanted α-C and oxidized functional groups over the graphene surface led to the degradation of the intrinsic graphene properties (see Figure S4 for detail nanostructure characterization). In addition to sample from the thermal decomposition method, Raman spectrum was taken on the sample prepared by the solvent replacing method(red spectrum in Figure 4a), where the α-C signal was not observed, and the crystallinity increased when it was further annealed to remove the residue PMMA(black spectrum in Figure 4a). Figure 4c shows SEM and TEM images for the suspended graphene prepared by the solvent replacing method. The result indicates a large amount of polymer residue on the graphene surface when it was treated only with acetone and solvent, while the additional thermal treatment significantly reduced the polymer to obtain a clearer graphene sample. The XPS analysis in Figure 4b shows a highly improved C/O ratio of 5.17, suggesting a lower content of carbon-

oxygen species on the surface. The aforementioned results clearly demonstrate that the suspended graphene quality, with respect to the crystallinity and cleanliness of the surface, was optimized by the solvent replacing method and subsequent thermal annealing.

Moreover, it is well-known that in the conventional graphene transferring process by employing an etching solution (such as $FeCl_3$) to remove the Cu substrate, residue metal iron/clusters were found to aggregate and distribute over the graphene surface. Figure 5a shows optical images for the 5L suspended graphene made by the $FeCl_3$ etching process followed by careful dilution with hydrochloride and DI-water for several times, which revealed a large amount of impurity on the surface. Further XPS characterization to obtain the Cu2p spectra indicates the existence of Cu metal residues on the graphene surface(Figure 5c). Employing the hydrogen bubbling transfer technique, as reported in a previous work,[32] can remarkably yield an extremely clean and metal-free graphene as shown in Figures 5b and c. The surface is uniform(approximately 5 nm in thickness over the membrane) and clean as shown by the AFM image in Figure 5d, suggesting that the bubbling transfer method provides a higher quality of suspended graphene membranes.

The aforementioned technique provides a reliable route to produce large-area suspended membranes down to a few atomic layers. This technology is not limited to substrates with holes and can be extended to substrates with more complex structures. Figure 6 shows the SEM images for a single-layered graphene suspended on a prefabricated substrate of an ordered array of Si nano-pillars, where the nano-pillars

having a height of 480 nm and a diameter of 103 nm were arranged with a pitch of 500 nm(Figure 6a). Figures 6 b and c show that the graphene can lay fully suspended over a length scale of 25 μm with minimal point contacts with the apexes of Si nano-pillars without collapse. Graphene supported onto the periodic arrays of pillars offers a unique platform to alter the stress in graphene layers where the strain domains are periodically arranged. The so-called strain superlattice in graphene was first reported in 2014 by designing specific geometries of pitch and density of nano-pillars array,[31] which was regarded as a promising strategy for engineering the electrical bandgap and optical conductivity of graphene due to the ripple-free features in graphene. However, the graphene collapse occurs during conventional transferring process, which obstructs the versatile design of the strain superlattice. Our proposed technique in this study can address this issue by fabricating a larger size of suspended graphene bridging over a large pitch between the pillars without collapsing. This leads to the potential applications of the strain superlattice, such as in high mobility nanoelectronics and photonic devices. Moreover, this unique structure might create a new platform to study new physical properties, such as electron/phonon transport on graphene, since the interaction from the substrate becomes minimal when the suspended graphene is altered by a point-like contact with periodic substrate interactions.

To examine the potential applications of the as-prepared ultra-large suspended graphene membranes, a capacitive pressure sensor based on the graphene membrane was first demonstrated in this investigation. Figure 7a illustrates the proof-of-concept for this device, where the graphene membrane was suspended across a quartz substrate with a circular hole(1.5 mm in diameter) and sealed in a small chamber. When gas

flows into the chamber, the induced deformation of the graphene membrane changes the capacitance between the fixed electrode and the graphene diaphragm. The real-time capacitance and chamber pressure were recorded by a LCR meter and pressure gauge. Figure 7b shows the optical images for the ballooned graphene membrane, and the largest deformation is approximately 100 μm(see Movie Clip 01 for the dynamic deformation of the membrane). In general, the performance of a capacitive pressure sensor could be according to the constructed model as shows below:

$$\frac{\Delta C}{P} = \frac{3(1-\upsilon^2)R^4}{16ET^3}\frac{\in_0 \in_r A_{sense}}{g^2}$$

where the ΔC= the change in capacitance, P= the pressure difference, R= radius of the diaphragm, T= thickness of the diaphragm, E= Young's modulus of the diaphragm material, υ= Poisson's ratio of the diaphragm material, $\varepsilon_0$= permittivity, $\varepsilon_r$= relative static permittivity, $A_{sense}$= the area of the moving plate, g= the sensing gap between the moving plate and the fixed plate. Therefore, in principle, the increased ratio of R/T resultant higher sensitivity.[30] The capacitance of the sensor is a function of the separation between the fixed electrode and the graphene membrane. When the graphene deforms close to the electrode, the capacitance increases and vice versa. The performance characterization of the capacitive pressure sensor is shown in Figure 7c, where the sensitivity was defined as the capacitance change per unit pressure difference(ΔC/ΔP).The curve revealed the linear characteristic for the pressure response. Moreover, the 5L graphene shows much better reliability and stability than 1L graphene film during the sensing operation. It was found out that the 5L graphene could sustain pressure difference(ΔP) up to 1800 Pa without rupturing. By controlling the limitation of pressure difference at less than 1900 Pa, the device shows excellent reliability and

long term stability at least up to ~200 cycles. Figure 7d compares the sensitivity obtained from this work to other conventional capacitive pressure sensors. The estimated sensitivity for the graphene-based pressure sensor is 15.2 aF/Pa, which is superior than the MEMS capacitive pressure sensors where the actuated diaphragms are composed of Cu/Si(1.7aF/Pa), Al/Si(2.9aF/Pa), and ultra-thin Si membranes(10aF/Pa), with thickness to diameter ratios of 25μm/1.2 mm, 25μm/572 μm, and 1.5μm/90μm, respectively. [33, 34] The results clearly indicate that the as-prepared macro-sized suspended graphene membrane exhibits a highly reversible elasticity than any other known thin-film material today because the graphene in this example shows an ultra-high aspect ratio of thickness to diameter of up to $3\times10^5$.Very recent works have demonstrated a wideband microphone and an ultrasonic radio made using multi-layered (~20 layers) suspended graphene as the diaphragm, which is beneficial for advanced communication technology in the future.[35] The large area graphene membrane with an ultra-high aspect ratio in this work shows excellent sensitivity and mechanical strength, which can be a potential candidate for the aforementioned applications in advanced communication.

In addition, the mechanical property of the graphene membrane is of great interest. Figure S5 shows the force curve for the suspended graphene membrane recorded by AFM. The resultant graphene still retained its strength and elastic properties without fracturing even at the deformation limit of the AFM tip of~5.5μm(see Movie Clip 02). Moreover, the highly elastic mechanical properties of the graphene membrane was studied, and the Q-factor under 2 MHz is measured to be 200-300 by a LCR meter. Although here we demonstrate the outstanding performance of the pressure sensor by

employing our ultra-large suspended graphene, it is believed that this technique could be readily applied to other versatile applications. For example in Figure S6,we demonstrate that the suspended graphene membrane is bridged over a long(~ 0.5 cm) trenched substrate($SiO_2$/Si) with a trench width of approximately 300μm. By employing the Hall measurement, the result shows that the hole carrier concentration for the suspended graphene is 37-fold lower than that of substrate-supported graphene samples, indicating the significantly reduced charge doping from the substrate. In addition, the normalized carrier mobility for the suspended graphene is 224% (2060 $cm^2$/vs on average) higher than that of substrate-supported graphene samples(920 $cm^2$/vs on average). This result showing the high carrier mobility in micro fluid trenches demonstrates the potential application in ultra-sensitive bio-sensors. Another example of utilizing suspended graphene is in highly sensitive touch or motion sensors (see Movie Clip 03), where the graphene membrane exhibits ultrafast response when subjected to knocking or environmental vibrations.

## Conclusion

In conclusion, we proposed a fabrication method to prepare an ultra-large area of high-quality suspended graphene membrane, where the stacking of 5L layers of graphene could be suspended across a circular hole with a diameter upto1.5 mm. The aspect ratio was $3x10^5$,which is a record for free-standing graphene membranes. The process is based on the growth of large crystalline graphene via CVD(~55μm), followed by a gradual solvent replacing technique. The utilization of a bubbling transfer approach and solvent replacement, as well as thermal annealing methods, led to the large-area and the extremely clean surface of the graphene membranes. A graphene-based capacitance

pressure sensor was first demonstrated, showing linear characteristics and a high sensitivity of 15.15 aF/Pa, which is 770% higher than that of conventional silicon-based membranes. The reported approach is universal on versatile substrates, such as arrays of Si nano-pillars and deep trenches. This work could not only pave a way for exploiting new physics/chemistry of intrinsic 2D layered materials but can also shed light on their potential applications in the future.

## Experimental Section:

***Synthesis of large single crystal graphene:***

Prior to the CVD growth process, the Cu foil(Alfa Aesar 99.8%; 25μm) was subjected to a surface flattening process by electrochemical polishing, where the Cu foil was placed in the anode and a Cu plate was employed as the cathode with a separation of 10 cm in an electrolyte mixture of 70 wt% $H_3PO_4$(Nihon Shiyaku 85%) with polyethylene glycol(Alfa Aesar, Polyethylene Glycol 6,000, PEG6,000) as additives. The optimized polishing time was 9 min(see FigureS1-1 and Table S1-2). The polished Cu-foil was then used as the substrate to synthesize graphene by the LPCVD method. The substrate was first loaded into a tubular furnace and was vacuumed to $5x10^{-3}$ Torr. The temperature was then ramped to 1060°C at a rate of 30℃/ min under a mixing gas of $H_2$/Ar(20/ 80 sccm), and the pressure was kept at 540 mTorr. The surface annealing process was carried out to reduce and flatten the Cu surface under a mixing gas of $H_2$/Ar(30/ 1000 sccm) at 760 Torr for 30 min. During the graphene growth process, the gas atmosphere was switched to $CH_4/H_2$/Ar (0.5/30/1000 sccm) at 760 Torr for 7 min. Then, it was cooled to room temperature under $H_2$/Ar(30/1000 sccm) flow to complete the process(see Figure S1-2 for detailed steps of the process).

***The transferring procedure for suspended graphene:***

The transferring process was based on the frequently used approach by spin coating(Step1: 500 rpm for 10 sec; Step2: 1000rpm for 60 sec) a supporting layer of poly(methyl methacrylate)(PMMA-A4, MicroCHEM) on the as-grown graphene/Cu substrate, followed by a baking step at 80°C for 5 min. The Cu substrate was etched away by 2 wt% ammonium persulfate (J.T. Baker), followed by placing it in a large amount of DI water to dilute the residue. The graphene/PMMA film was transferred onto the target substrate(another graphene/Cu substrate), and then it was immediately dried by high speed spinning (Step1: 500 rpm for 10 sec, and step2: 1000rpm for 60 sec) to remove the water film between the graphene/PMMA and the substrate followed by baking at 80°C for 10 min. To release the internal strain, a reflow process was carried out by dropping PMMA on the surface and drying. The sample was immersed into warm acetone for 10 min to remove the PMMA. Then, it was loaded into a furnace for thermal annealing under $H_2$/Ar(20/80 sccm) at 450°Cfor 40 min. A 5 layered graphene was realized by repeating the layer-by-layer stacking approach according to the aforementioned procedures. The Si nano-pillar substrates were prepared by electron beam lithography, followed by the reactive iron etching(RIE) process.

To obtain the large area suspended graphene samples, Cu/5L-graphene/PMMA was subjected to an etching step to remove the Cu followed by DI water cleaning; then, it was transferred to a substrate with a hole (e.g., stainless steel plate of 500 μm in thickness with arrays of holes ranging from 20 μm to 1.5 mm in diameter) and dried at 80°C for 10 min. The bubbling transfer process was another method we employed, where the graphene/PMMA layers were delaminated from the Cu substrate by an

electrochemical method in a 1 M NaOH solution, and the voltage bias was constant at 2.3 V.

The most important step was to remove the PMMA supporting layer. Here, the substrate was placed upside down across two glass slides (2 mm in thickness). The acetone was streamed as a gentle flow through the underlying channel and fully contacted the graphene/PMMA surface by controlling the flow rate at 1.7 mL/s with a peristaltic pump for 10 min. Then, the acetone was replaced by a low surface tension solvent, i.e., $C_4F_9OCH_3$ (3 M, Novec 7100), to remove the acetone residue and subsequently dried in atmosphere. Finally, the sample was loaded into a furnace for an additional annealing step under $H_2$/Ar(20/80 sccm) at 450°C under 540 mTorr for 40 min. The direct thermal decomposition method also followed the same annealing conditions.

***The fabrication and characterization of capacitive pressure sensor device:***

To fabricate the pressure sensor, the 5L-graphene membrane was transferred onto a quartz substrate with a 1.5 mm diameter hole. The substrate was then bonded onto a glass substrate, where the spacing between the quartz and the glass was adjusted to be 80 μm by a spacer tape. The edge of the sample was carefully sealed by silicone gel to prevent gas leakage from the edges. The gas inlet pipe(500 μm in diameter) and pressure gauge were integrated on the device, where a gas flow rate of 3.3 μL/s was controlled. To measure the response of the pressure sensor, a Cu electrode was placed above the suspended graphene membrane at a distance of 160μm. The capacitance was measured by a voltage ranging from -40 V to 40 V with a stimulated frequency of 20 Hz ～2 MHz in an Agilent electrical meter(E4980A).

***Material characterizations:***

AFM was performed using a Bruker Innova system to characterize the thicknesses of the as-prepared multi-layered graphene films. Raman scattering spectral analysis were collected using a Horiba HR 550 confocal Raman microscope system (laser excitation wavelength = 532 nm; laser spot-size ~ 0.5 μm). The Raman scattering peak of Si at 520 $cm^{-1}$ was used as a reference for wavenumber calibration. The chemical configurations were determined using an X-ray photoelectron spectrometer (XPS, Phi V6000). The XPS measurements were performed using an Mg Kα X-ray source for sample excitation. The energies were calibrated relative to the C1s peak to eliminate charging of the sample during analysis. SEM wascarried out in a JEOL-6330F, and TEM observation was carried out in a JEOL-2010F with an accelerating voltage of 200keV. Electrical conductivity, carrier concentration and mobility measurement were carried out on a Hall measurement system(Swin HALL8800). UV-vis-NIR transmittance spectra were obtained using a spectrophotometer(Jasco V670).

**Supporting Information Available**: The detailed process/recipe for CVD-grown graphene and the transferring process, SEM, TEM, contact angles, force curves, and movie clips are available on RSC or from the author.

**Acknowledgements:** This research was supported by the Ministry of Science and Technology, Taiwan (102-2221-E-008-113-MY3). JL acknowledges support by NSF CBET-1240696andDMR-1120901.

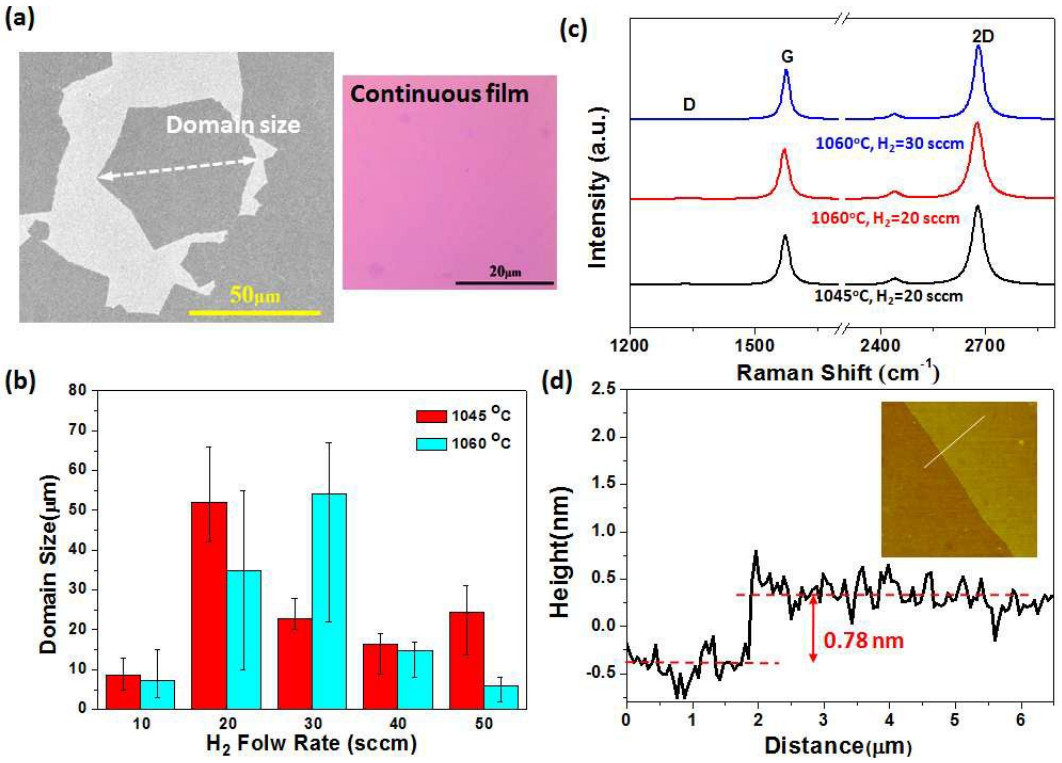


**Figure 1.**(a)Typical SEM image of the single-crystalline graphene domains grown by APCVD. The right image is an optical image for the continuous graphene film that was transferred onto a $SiO_2$/Si substrate. (b) Statistical analysis on the graphene domain sizes for various growth conditions, showing that a relatively larger domain size could be obtained by the following conditions: 1045˚C($H_2$ 20 sccm) and 1060˚C($H_2$ 20 sccm) and 1060°C($H_2$ 30 sccm).(c) Typical Raman spectra for these three samples. (d) AFM height profile for the samples prepared under the condition of 1060°C($H_2$ 30 sccm), indicating a uniform thickness of 0.78 nm.

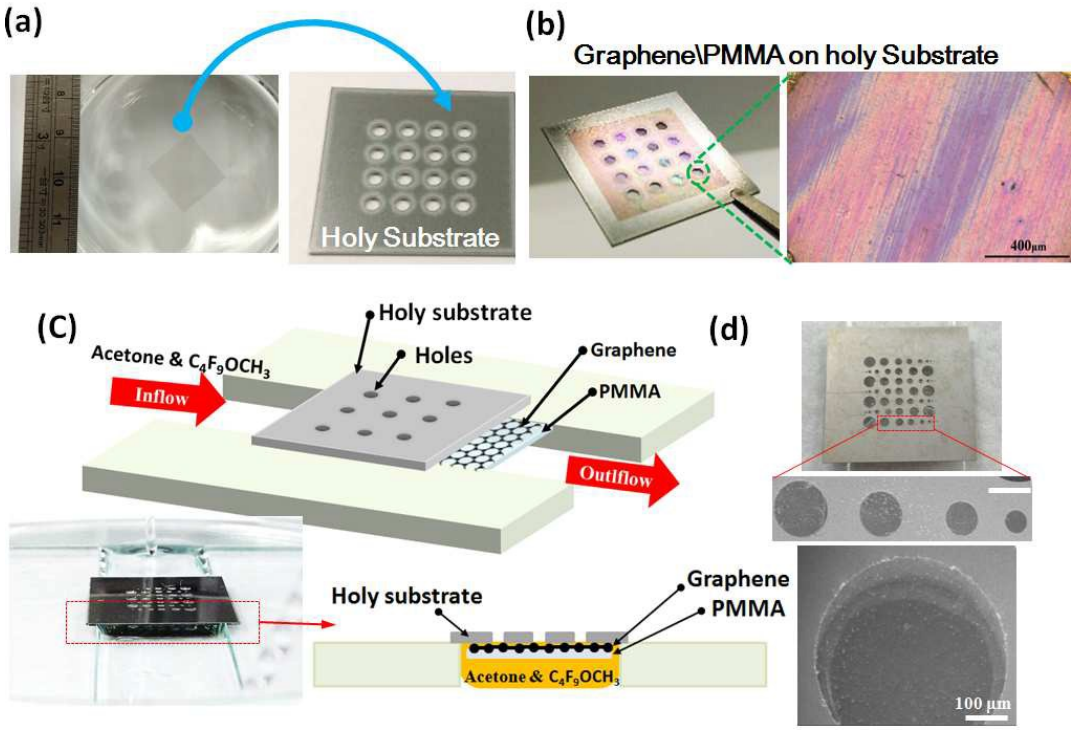


**Figure 2.**Thetransferring procedures for fabricating ultra-large suspended graphene membranes**.** (a)The optical images for aPMMA/graphene composite film floating on the water surface and receiving a stainless steel substrate with holes. (b) The PMMA/graphene composite film was transferred onto the substrate with holes without rupturing. (c) Schematic illustration of the procedures for the solvent replacing method, where pristine graphene membrane could be well-suspended across the substrate with holes without rupturing when PMMA was removed and dried by a low surface tension solvent. (d) Optical and SEM images of graphene successfully suspended over circular holes of 600μm~ 1200μm in diameter. The scale bar is 1mm.

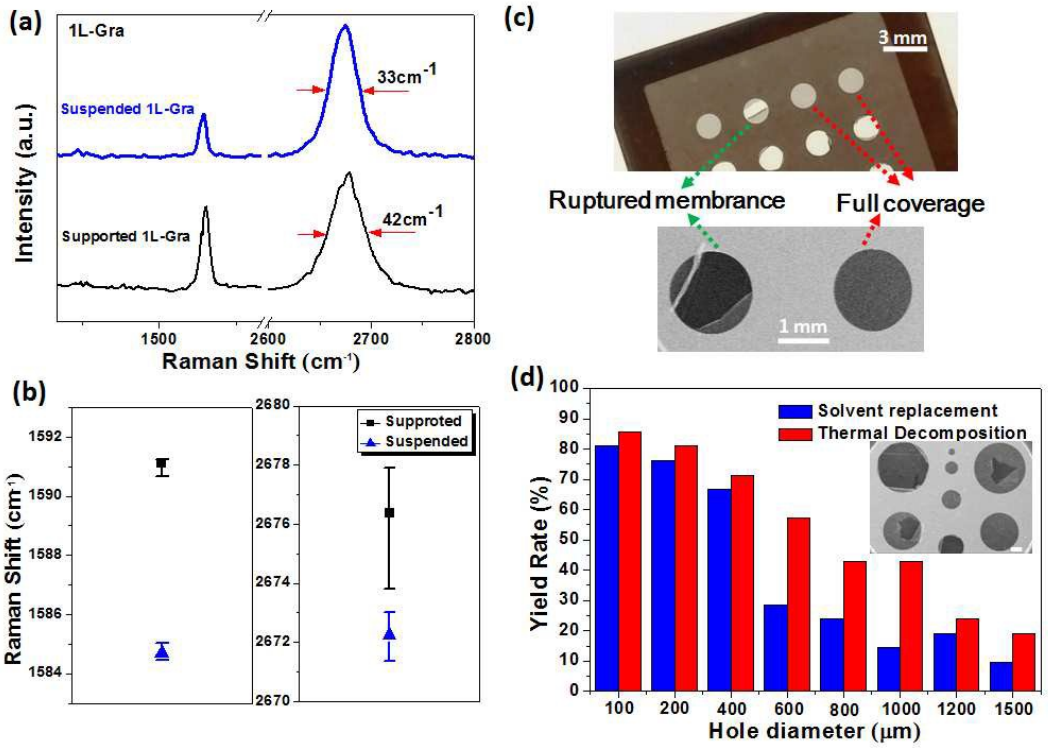


**Figure 3.** (a) Comparison of the typical Raman feature peaks(G and 2D) for the cases of the substrate-supported single-layered (1L-) graphene and the suspended 1L-gaphene membrane. (b) The corresponding peaks positions of G and 2D peaks for the substrate-supported and suspended graphene samples. (c) The optical and SEM images for the ruptured and fully coverage graphene membrane on the substrate with 1.5mm diameter holes. (d) Histogram of the statistical yield rate for the various hole diameters by the solvent replacing and thermal decomposition method, respectively. The inset shows the SEM images for testing samples(scale bar is 300 μm), where the yield is defined as the fully coverage of membrane without any cracks or ruptures.

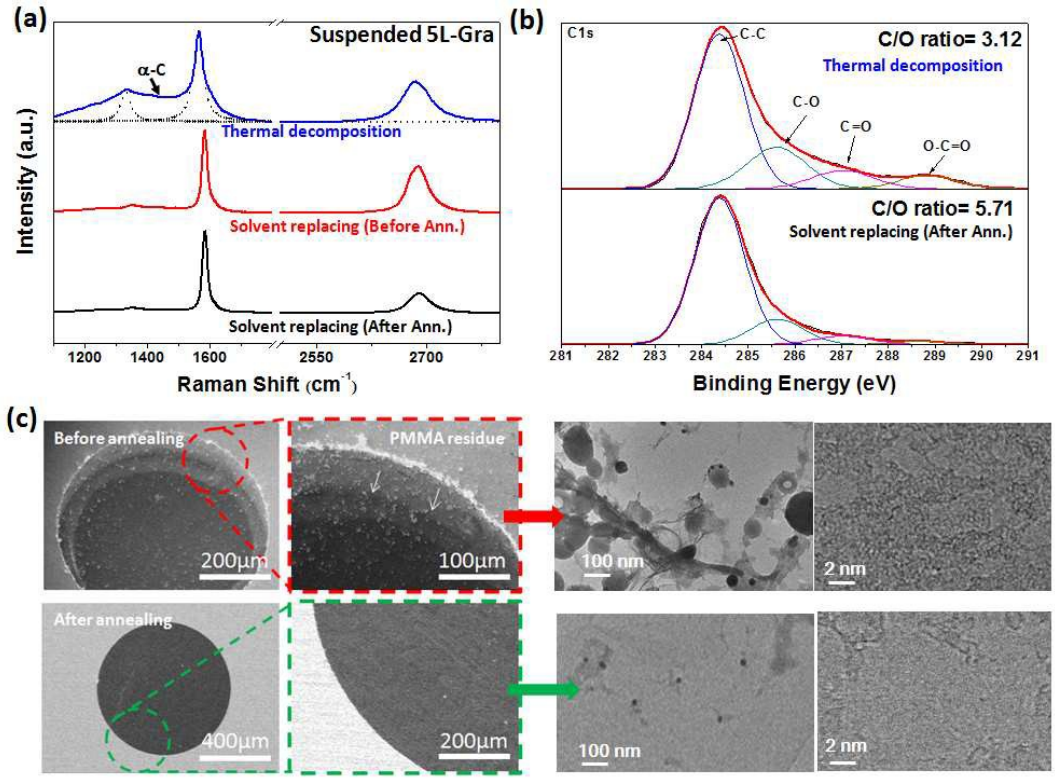


**Figure 4.(a)** Raman spectra for the suspended 5L graphene membranes made by three approaches, i.e., thermal decomposition and solvent replacing methods with/without post-annealing. (b) Comparison of the XPS C1s spectra for the graphene membranes made by solvent replacement with/without post-annealing. (c) Comparison of surface morphologies and nanostructures by SEM and HRTEM for samples with/without post-annealing, indicating the efficient removal of PMMA residue(denoted by white arrows) when subjected to post-annealing.

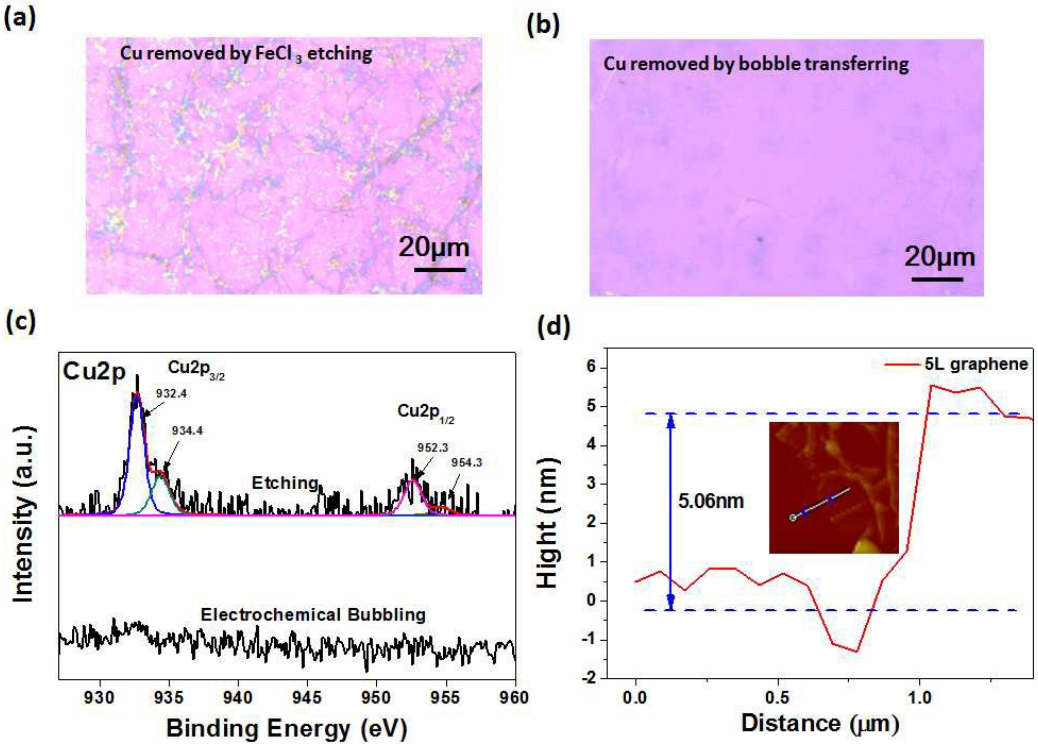


**Figure 5.**Typical optical images for the 5L graphene samples prepared by (a) conventional Cu etching and (b) bubbling transfer method. (c) The corresponding XPS Cu2p spectra for these two graphene membranes. (d) AFM image and height profile for the samples by the bubbling transfer method.

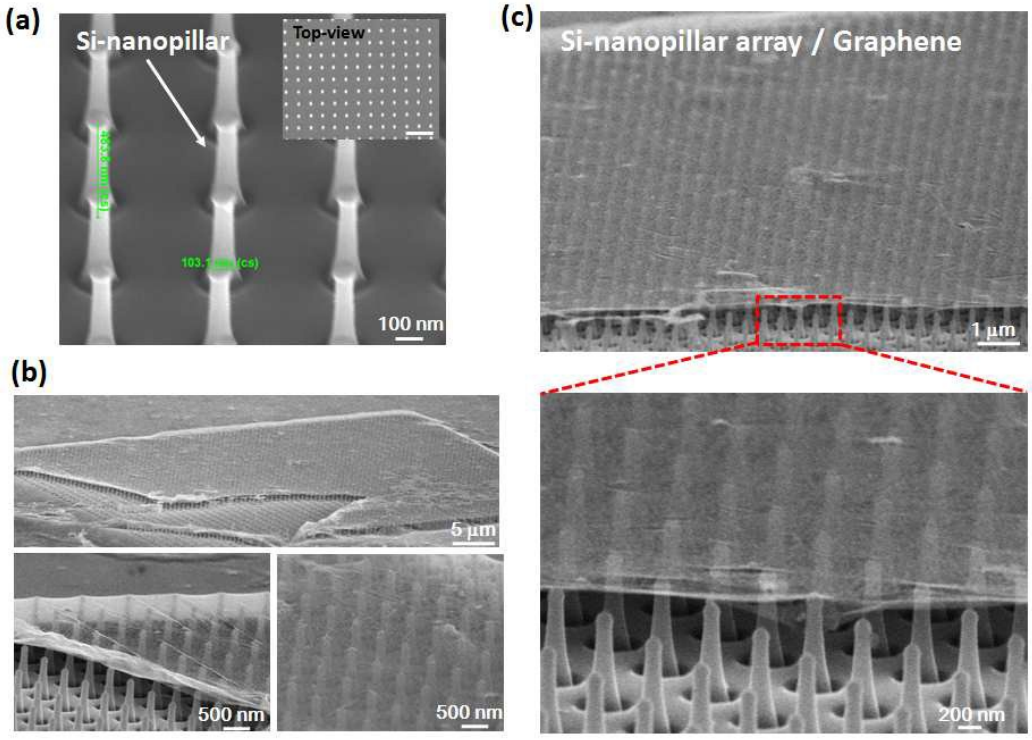


**Figure 6.**A single-layered graphene membrane suspended on a prefabricated substrate of an ordered array of Si nano-pillars. (a) SEM images for the fabricated Si nano-pillars. The inset shows a top-view image of the substrate(scale bar: 1μm). (b) Images for the suspended graphene over a macro-size of 25μm. (c) Magnified images of the nano-pillar supported graphene, showing a uniform and wrinkle-free surface.

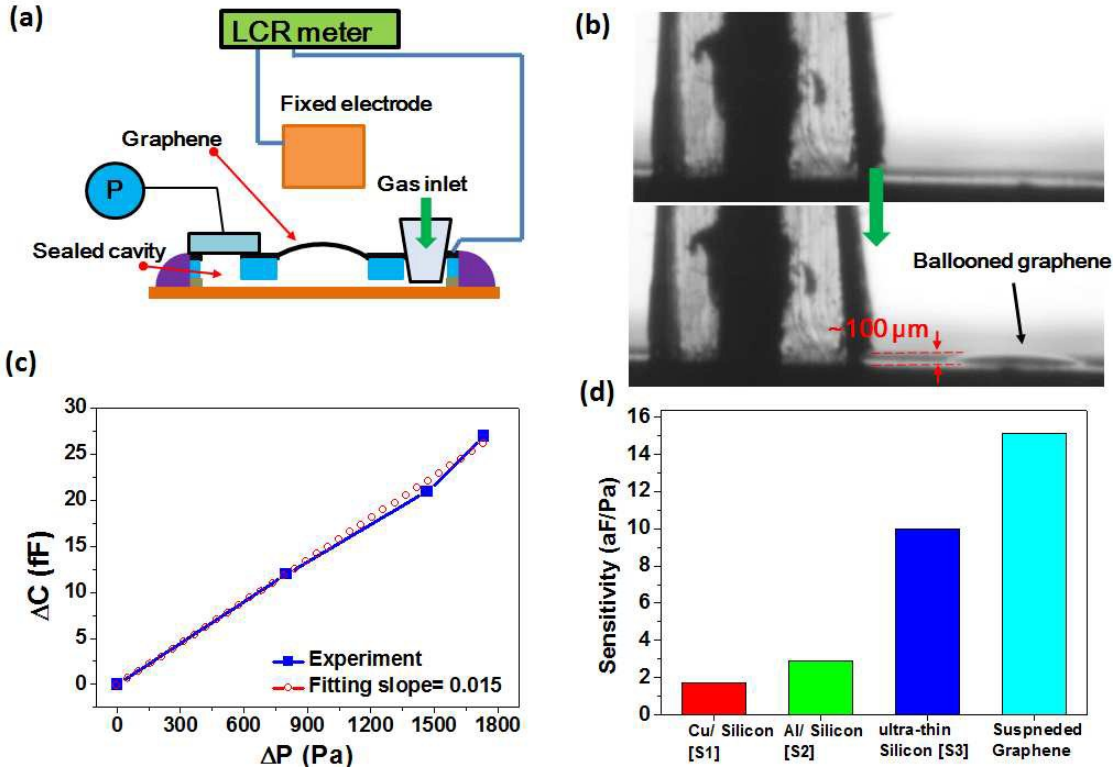


**Figure 7.**Application of graphene-based capacitive pressure sensor. (a) Illustration of the scheme of the sensor design and setup. A LCR meter was used for the real-time recording of capacitance variation.(b) Optical images of the ballooned graphene membrane when the gas flowed into the chamber, where the suspended diameter is 1.5 mm and the estimated deformation is ~ 100 μm. (c) The correlation of capacitance change and measured pressure variations; the sensitivity was defined as $\Delta C/\Delta P$. (d) Histogram of the sensitivity for this work compared to other conventional capacitive pressure sensors made using Cu/Si, Al/Si, and ultra-thin Si membranes (denoted S1-S3[33, 34] ) by MEMS technologies.

# References


1. K. E. Mueggenburg, X.-M. Lin, R. H. Goldsmith and H. M. Jaeger, *Nat Mater*, 2007, **6**, 656-660.
2. J. He, P. Kanjanaboos, N. L. Frazer, A. Weis, X.-M. Lin and H. M. Jaeger, *Small*, 2010, **6**, 1449-1456.
3. K. C. Ng, I. B. Udagedara, I. D. Rukhlenko, Y. Chen, Y. Tang, M. Premaratne and W. Cheng, *ACS Nano*, 2012, **6**, 925-934.
4. Y. Chen, Z. Ouyang, M. Gu and W. Cheng, *Advanced Materials*, 2013, **25**, 80-85.
5. W. Cheng, M. J. Campolongo, J. J. Cha, S. J. Tan, C. C. Umbach, D. A. Muller and D. Luo, *Nat Mater*, 2009, **8**, 519-525.
6. K. S. Novoselov, A. K. Geim, S. V. Morozov, D. Jiang, Y. Zhang, S. V. Dubonos, I. V. Grigorieva and A. A. Firsov, *Science*, 2004, **306**, 666-669.
7. K. I. Bolotin, K. J. Sikes, Z. Jiang, M. Klima, G. Fudenberg, J. Hone, P. Kim and H. L. Stormer, *Solid State Communications*, 2008, **146**, 351-355.
8. C. Lee, X. Wei, J. W. Kysar and J. Hone, *Science*, 2008, **321**, 385-388.
9. A. A. Balandin, S. Ghosh, W. Bao, I. Calizo, D. Teweldebrhan, F. Miao and C. N. Lau, *Nano Letters*, 2008, **8**, 902-907.
10. W. Bao, F. Miao, Z. Chen, H. Zhang, W. Jang, C. Dames and C. N. Lau, *Nature Nanotechnology*, 2009, **4**, 562-566.
11. K. V. Zakharchenko, M. I. Katsnelson and A. Fasolino, *Physical Review Letters*, 2009, **102**.
12. J. C. Meyer, A. K. Geim, M. I. Katsnelson, K. S. Novoselov, T. J. Booth and S. Roth, *Nature*, 2007, **446**, 60-63.
13. C. N. Lau, W. Bao and J. Velasco, Jr., *Materials Today*, 2012, **15**, 238-245.
14. J. S. Bunch, A. M. van der Zande, S. S. Verbridge, I. W. Frank, D. M. Tanenbaum, J. M. Parpia, H. G. Craighead and P. L. McEuen, *Science*, 2007, **315**, 490-493.
15. P. Li, B. Zhang and T. Cui, *Biosens. Bioelectron.*, 2015, **72**, 168-174.
16. B. M. Venkatesan and R. Bashir, *Nat Nano*, 2011, **6**, 615-624.
17. A. D. Smith, F. Niklaus, A. Paussa, S. Vaziri, A. C. Fischer, M. Sterner, F. Forsberg, A. Delin, D. Esseni, P. Palestri, M. Ostling and M. C. Lemme, *Nano Letters*, 2013, **13**, 3237-3242.
18. Y. D. Kim, H. Kim, Y. Cho, J. H. Ryoo, C.-H. Park, P. Kim, Y. S. Kim, S. Lee, Y. Li, S.-N. Park, Y. Shim Yoo, D. Yoon, V. E. Dorgan, E. Pop, T. F. Heinz, J. Hone, S.-H. Chun, H. Cheong, S. W. Lee, M.-H. Bae and Y. D. Park, *Nature nanotechnology*, 2015, **10**, 676-681.
19. M. Freitag, T. Low and P. Avouris, *Nano Letters*, 2013, **13**, 1644-1648.
20. J. S. Bunch, S. S. Verbridge, J. S. Alden, A. M. van der Zande, J. M. Parpia, H. G. Craighead and P. L. McEuen, *Nano Letters*, 2008, **8**, 2458-2462.
21. K. Celebi, J. Buchheim, R. M. Wyss, A. Droudian, P. Gasser, I. Shorubalko, J.-I. Kye, C. Lee and H. G. Park, *Science*, 2014, **344**, 289-292.
22. J. M. Yuk, J. Park, P. Ercius, K. Kim, D. J. Hellebusch, M. F. Crommie, J. Y. Lee, A. Zettl and A. P. Alivisatos, *Science*, 2012, **336**, 61-64.

23. C. Wang, Q. Qiao, T. Shokuhfar and R. F. Klie, *Advanced Materials*, 2014, **26**, 3410-3414.
24. J. Park, H. Park, P. Ercius, A. F. Pegoraro, C. Xu, J. W. Kim, S. H. Han and D. A. Weitz, *Nano Letters*, 2015, **15**, 4737-4744.
25. S. Buckhout-White, J. T. Robinson, N. D. Bassim, E. R. Goldman, I. L. Medintz and M. G. Ancona, *Soft Matter*, 2013, **9**, 1414-1417.
26. K. Kim, Z. Lee, W. Regan, C. Kisielowski, M. F. Crommie and A. Zettl, *ACS Nano*, 2011, **5**, 2142-2146.
27. P. Y. Huang, C. S. Ruiz-Vargas, A. M. van der Zande, W. S. Whitney, M. P. Levendorf, J. W. Kevek, S. Garg, J. S. Alden, C. J. Hustedt, Y. Zhu, J. Park, P. L. McEuen and D. A. Muller, *Nature*, 2011, **469**, 389-392.
28. P. Li, B. Zhang and T. H. Cui, *Biosens. Bioelectron.*, 2015, **72**, 168-174.
29. C.-K. Lee, Y. Hwangbo, S.-M. Kim, S.-K. Lee, S.-M. Lee, S.-S. Kim, K.-S. Kim, H.-J. Lee, B.-I. Choi, C.-K. Song, J.-H. Ahn and J.-H. Kim, *ACS Nano*, 2014, **8**, 2336-2344.
30. Y. Zhang, R. Howver, B. Gogoi and N. Yazdi, 2011.
31. A. Reserbat-Plantey, D. Kalita, Z. Han, L. Ferlazzo, S. Autier-Laurent, K. Komatsu, C. Li, R. Weil, A. Ralko, L. Marty, S. Guéron, N. Bendiab, H. Bouchiat and V. Bouchiat, *Nano Letters*, 2014, **14**, 5044-5051.
32. L. Gao, W. Ren, H. Xu, L. Jin, Z. Wang, T. Ma, L.-P. Ma, Z. Zhang, Q. Fu, L.-M. Peng, X. Bao and H.-M. Cheng, *Nat Commun*, 2012, **3**, 699.
33. S. Saleh, A. Zaki, H. Elsemary and S. Ahmad, 2006.
34. Y. H. Wu and C. H. Chien, Thesis for Master of Science, Tatung University, 2008.
35. Q. Zhou, J. Zheng, S. Onishi, M. F. Crommie and A. K. Zettl, *Proceedings of the National Academy of Sciences*, 2015, **112**, 8942-8946.